Homoepitaxial growth of Bi(111)

G. Jnawali,* H. Hattab, C. A. Bobisch,† A. Bernhart, E. Zubkov, R. Möller, and M. Horn-von Hoegen
Department of Physics and Center for Nanointegration Duisburg-Essen (CeNIDE), University of Duisburg-Essen, Lotharstr. 1, 47057 Duisburg, Germany

(Received 21 April 2008; revised manuscript received 14 May 2008; published 21 July 2008)

Homoepitaxial growth of Bi(111) at temperatures between 80–300 K has been studied using spot profile analyzing low-energy electron diffraction (SPA-LEED) and scanning tunneling microscopy (STM). From the intensity oscillations of the (00)-spot with Bi coverage and the STM topography of two-dimensional (2D) islands at low coverage, a pure 2D nucleation followed by a quasi bilayer-by-bilayer growth mode has been confirmed. The oscillation amplitude decays slowly with coverage, indicating a slow kinetic roughening due to a weak *Ehrlich-Schwoebel* step edge barrier. From the Arrhenius behavior of the average island separation an intraterrace diffusion barrier of E_d=0.135 eV is estimated. Regularly ordered quasidendritic shape islands reflect an asymmetry in adatom diffusion along the steps and the corners of the islands.

DOI: 10.1103/PhysRevB.78.035321 PACS number(s): 68.55.A−, 68.37.Ef, 61.05.jh

I. INTRODUCTION

The semimetal bismuth (Bi) has been extensively studied in the past few decades, due to its unique transport properties.[1] Since 1999, when Yang *et al.*[2] observed very large magnetoresistance (MR) effects in single crystalline Bi films, which is the key to realizing spintronic devices such as magnetic-field sensing,[3] the interest in Bi films is rapidly growing. As more techniques are emerging to produce high quality ultrathin Bi films, surface effects start to play an important role in transport properties. The observation of spin-orbit splitting in highly metallic Bi surface states[4–7] and large surface state conductivity in ultrathin Bi films[8] has further extended the possibility of using Bi films in spin-based device applications.

In the context of the growing interest in Bi films, a microscopic understanding of the growth mechanism becomes more relevant. In the case of heteroepitaxy, an earlier study has shown that Bi(111) grows commensurately on Si(111)-7×7 substrates with the occurrence of the so-called "magic mismatch" between both lattices, resulting in a high quality film.[9,10] In a recent study, we have shown that a Bi(111) lattice also fits well on Si(001) substrates.[11] A remaining lattice mismatch of 2.3% is accommodated via the formation of a periodic dislocation network at the interface.[12] This recipe allows the production of relaxed Bi(111) films with an extremely smooth surface.[11,13] In both cases, an understanding of the microscopic lattice accommodation has been exclusively discussed. However, until now, nothing is known about the homoepitaxial growth of Bi(111) films, which is equally important in understanding the complete picture of the growth mechanism of Bi heterofilms.

Homoepitaxial growth at low temperatures is controlled by kinetic processes such as deposition, the diffusion of atoms on the surface and the nucleation of islands. According to the Venables nucleation theory[14,15] the growth processes are determined by both external parameters such as the deposition rate and the growth temperature, and internal parameters such as intralayer and interlayer diffusion barriers. With a careful measurement of the film morphology at different growth conditions, the internal parameters can be determined. The intralayer diffusion energy E_d can be estimated from the island density n_x for different deposition temperatures at constant deposition rate and coverages.[16]

Many techniques, such as field ion microscopy (FIM),[17] scanning tunneling microscopy (STM),[18,19] or reflection high-energy electron diffraction (RHEED)[20,21] have been used previously to estimate the activation energy for surface diffusion. Among them, diffraction is highly appreciated and considered a convenient technique, which has also the advantage to provide information of the surface morphology evolution during deposition.[22–24] Its excellent averaging property of large and representative surface areas offers a superior statistics for data analysis. Unlike real imaging techniques such as STM, which give a direct evaluation of the island density, diffraction techniques provide information about the average island separation $\langle L\rangle$ or the average island size $\langle\Gamma\rangle$ on the surface. Since the average island separation is directly related to the island density n_x via $\langle L\rangle \sim n_x^{-1/2}$ at the submonolayer regime,[25] both parameters can be used to calculate the diffusion energy.

In this paper, we present results on two-dimensional (2D) layer growth during the deposition of Bi on a Bi(111) film at various temperatures between 80 and 300 K. Spot profile analyzing low-energy electron diffraction (SPA-LEED)[23] is used to characterize the surface morphology *in situ* during deposition and afterward. The average island separation $\langle L\rangle$, has been calculated from the diameter of the diffuse intensity in the diffraction profile. As a complementary check, STM was used to obtain real-space information of the island shape and density at 135 K. The Venables nucleation theory[14,15,26] was applied to determine the intraterrace diffusion energy supposing a critical nucleus size of one (single atom).

II. EXPERIMENT

The measurements were performed in an ultrahigh vacuum (UHV) chamber with a base pressure better than 2×10^{-10} mbar. The chamber is equipped with a SPA-LEED system,[23,27] which was used at normal incidence to analyze the surface morphology after deposition. The change of the surface morphology during deposition was studied using SPA-LEED in a RHEED-like geometry. Highly oriented Si(001) samples (Boron doped, resistivity=8–12 Ω cm) with a dimension of $(3.5\times0.4\times0.05)\text{cm}^3$ were degassed at

870 K for 12 h prior to a short flash annealing to 1470 K by direct current heating. This process removes the native oxide and results in a clear (2×1) low-energy electron diffraction (LEED) pattern at room temperature indicating a clean and defect-free surface. The sample was cooled down to 80 K by using a liquid nitrogen cryostat attached to the sample holder. Intermediate temperatures were achieved by heating the sample by radiation from a tungsten filament attached to the temperature controller system. The observation of clear and sharp $c(4\times2)$ LEED spots of the Si(001) surface at temperatures below 200 K indicates a clean surface undergoing the reversible order-disorder phase transition from (2×1) to $c(4\times2)$ reconstruction at low temperatures.[28–31]

Prior to every experiment, a high quality Bi(111) base film was prepared on a Si(001) substrate following a recipe described by Jnawali *et al.*,[11] which results in extremely smooth Bi(111) surfaces with large terraces.[13] The deposition of high-purity Bi (Purity=99.9999%) was carried out by thermal evaporation from a directly heated ceramic crucible mounted in a water-cooled copper shroud. During the deposition process, the residual pressure was better than 4×10^{-10} mbar. A deposition rate of 0.6 bilayer/minute (or BL/min) (1 BL=1.14×10^{15} cm^{-2}) was maintained during each deposition process. The deposition rate was monitored by a quartz microbalance mounted to the evaporator. A precise thickness calibration was obtained from BL intensity oscillations of the (00)-spot with coverage during Bi deposition on the Bi(111) base film as shown in Fig. 1.

All LEED patterns and LEED spot profiles were recorded at 80 K and are presented in a logarithmic intensity scale.

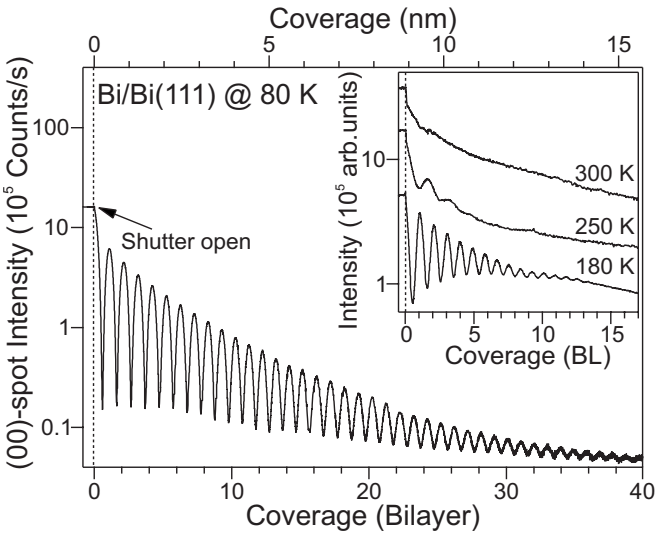

FIG. 1. LEED specular beam, i.e., (00)-spot intensity oscillations measured at an out-of-phase condition ($S=3.5$) during deposition of Bi on Bi(111) base film at 80 K. Long-lasting oscillations with a period of bilayer coverage confirm a quasibilayer growth mode. The gradual decay of the oscillation amplitude reflects a kinetic roughening of the growth front. The inset shows the intensity oscillations at higher deposition temperatures.

The diffraction conditions for the (00)-spot were chosen by varying the scattering phase $S=k_\perp d/2\pi$, where $k_\perp$ is the component of the electron momentum transfer perpendicular to the surface and d is the interlayer spacing of Bi(111) film

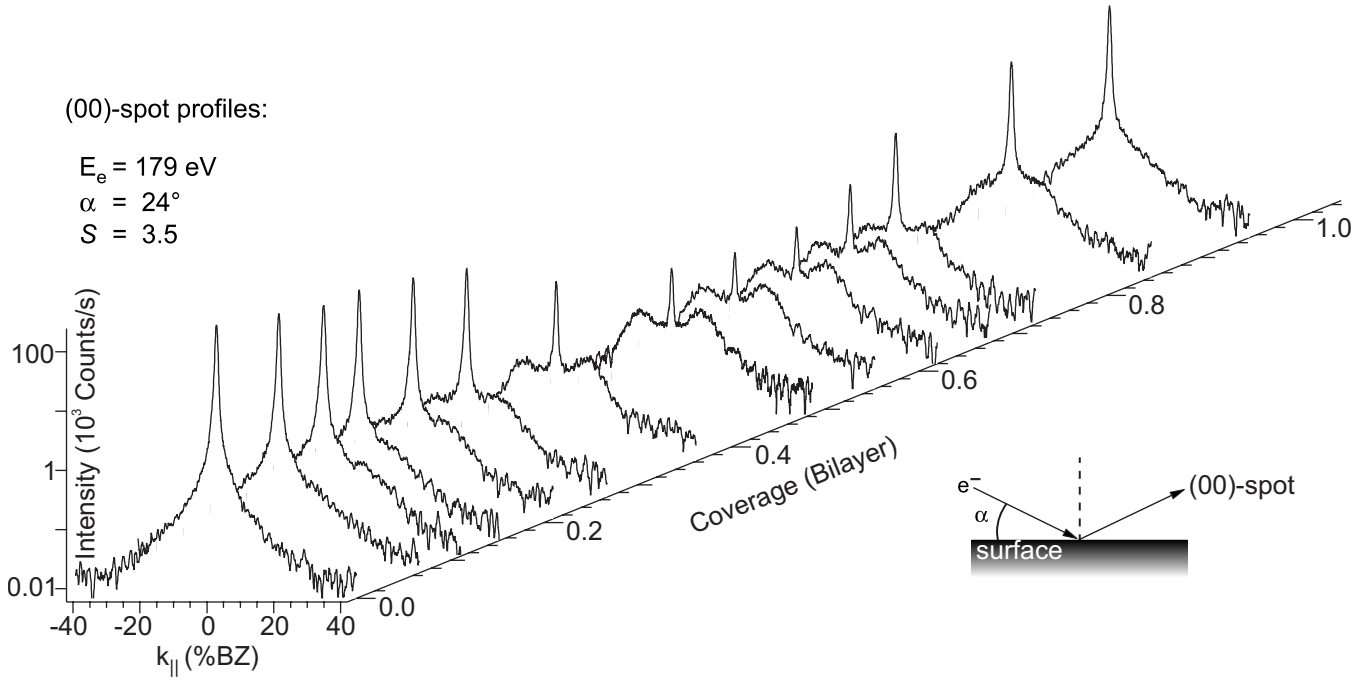

FIG. 2. (00)-spot profiles recorded at an out-of-phase condition ($S=3.5$) during the deposition of Bi on a Bi(111) base film at 80 K. The shape of the profile changes periodically with coverage. The sharp central spike $G(S)$ recovers from one complete bilayer to the next complete bilayer, indicating a 2D growth mode. At 0.5 BL coverage, the profile shows a pronounced diffuse shoulder with a sharp central peak, reflecting a surface roughness with a well-defined average terrace separation of $\langle L\rangle=4.6$ nm. The total intensity of the diffuse shoulder and the central spike is conserved during the morphological changes during deposition. The profiles were measured using an electron beam in a RHEED-like geometry as shown in the sketch (below the profiles).

(bulk value $d_{\text{bulk}}=0.394$ nm). For an integral scattering phase $S=n$, a Bragg- or in-phase condition is observed, for $S=n+\frac{1}{2}$ an anti-Bragg- or out-of-phase condition. Since electrons interfere constructively at an in-phase condition, they are not sensitive to the surface roughness. In contrast, electrons interfere destructively at an out-of-phase condition and are most sensitive to steps at the surface. Therefore, all the LEED spots and corresponding spot profiles were recorded at an out-of-phase condition.

Because the activation energy for intralayer diffusion does not depend on the (submonolayer) coverage,[32] half of a Bi-BL was always deposited in order to obtain spot profiles from the diffuse intensity, which are not outshined by a strong central spike. The parallel scattering vector $k_{\|}$ will be expressed in percent units of the first Brillouin zone (%BZ) of Bi(111) along $[11\bar{2}]$ direction, where 100%BZ corresponds to the reciprocal lattice vector of the Bi(111) surface, i.e., $2\pi/[a_{\text{Bi(111)}}\sin 60°]$ with $a_{\text{Bi(111)}}=0.454$ nm.

The island topography was additionally studied by STM in a separate UHV chamber. The sample was cleaned and the Bi(111) base films were prepared using the same procedure as for the SPA-LEED measurements. The topography was recorded after a deposition of 0.5 BL Bi on top of the base film at 135 K.

III. RESULTS AND DISCUSSION

A. Growth mode at low temperature

Figure 1 shows the (00)-spot intensity during the deposition of Bi on Bi(111) at 80 K. An electron energy of 179 eV was chosen as an out-of-phase condition where electrons interfere destructively after scattering from neighboring terraces. The intensity shows an oscillatory dependence on coverage. This clearly reflects a quasi layer-by-layer growth mode. We will show later that all the 2D islands exhibit a bilayer height of 0.394 nm: the growth proceeds in a bilayer-by-bilayer fashion. At the very beginning of the coverage, we have observed an initial transient in the intensity, which is caused by the scattering of the electron wave by isolated adatoms.[33] The intensity of the periodic maxima is significantly lower than those originating from the initial surface. The maxima exhibit rounded peaks. This is easily explained by the nucleation of a new layer before the previous one is completed.[34] Moreover, the amplitude of the oscillation monotonously decreases from layer to layer. Typically 40 oscillations have been observed at 80 K (Fig. 1) which finally fade out at higher coverage. The decay of the oscillation amplitude is a clear evidence of kinetic roughening of the growth front. We attribute this to the existence of a weak *Ehrlich-Schwoebel* step edge barrier,[35,36] which becomes less effective at higher temperatures forcing the growth mode toward step-flow propagation. The shift of the growth mode can be clearly observed in the (00)-spot intensity variation at higher temperatures in the inset of Fig. 1. The oscillation amplitudes are drastically reduced at 250 K and completely turned off at 300 K. Since the (00)-spot intensity at 300 K does not show constant behavior with the coverage, which is a prerequisite for perfect step-flow propagation, a slight roughening is still present.

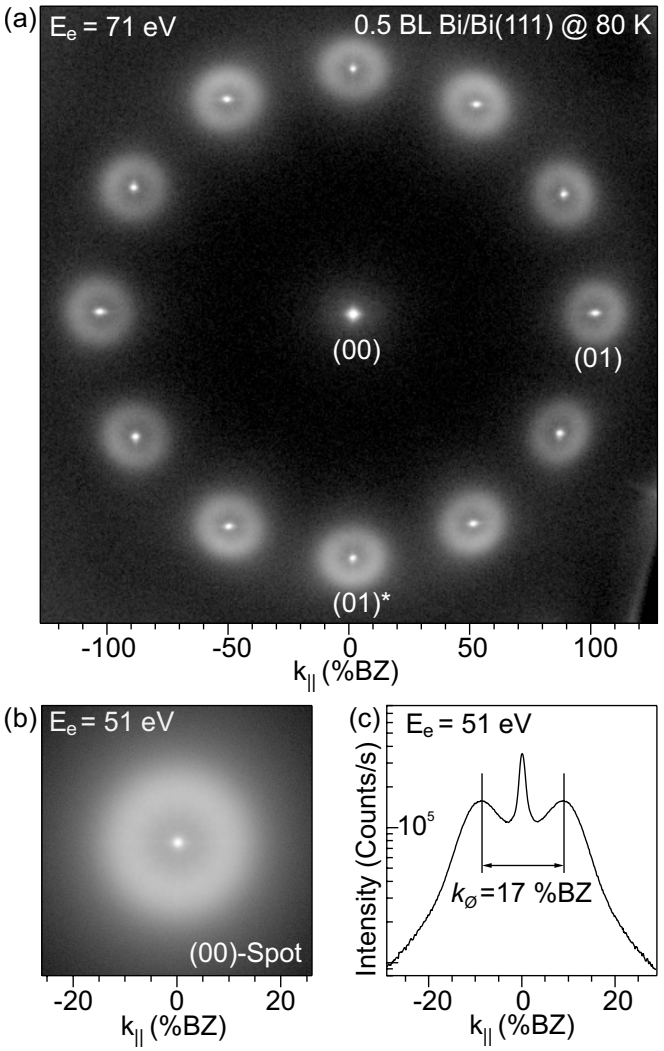

FIG. 3. LEED pattern of Bi(111) surface after deposition of 0.5 BL Bi at 80 K: (a) First-order LEED spots close to the out-of-phase condition ($S=5.4$). (b) LEED pattern of the (00)-spot close to the out-of-phase condition ($S=4.5$). (c) Corresponding profile of the (00)-spot. Both the (00)-spot and the first-order spots exhibit a ring of diffuse intensity surrounding a sharp central peak showing a typical Henzler ring.

Nevertheless, the observation of long-lasting oscillations at low temperatures is quite rare in metallic homoepitaxial systems because thermally activated surface diffusion is effectively suppressed and hinders 2D growth. However, as suggested by Egelhoff *et al.*,[33] adatoms may use their latent heat of condensation to hop across the surface and finally come to rest at growing island edges.

The behavior of the (00)-spot intensity can be understood from the periodic variation of the (00)-spot profile during deposition. Figure 2 shows a series of (00)-spot profiles recorded at an out-of-phase condition ($S=3.5$) during deposition. The variation of the spot profiles clearly demonstrate the oscillating behavior of the central spike intensity and of the diffuse intensity (which is phase shifted by half a BL) from one bilayer to the next one. The total intensity of the profile is always conserved. The periodic change of the profile reflects the nucleation and the completion during the

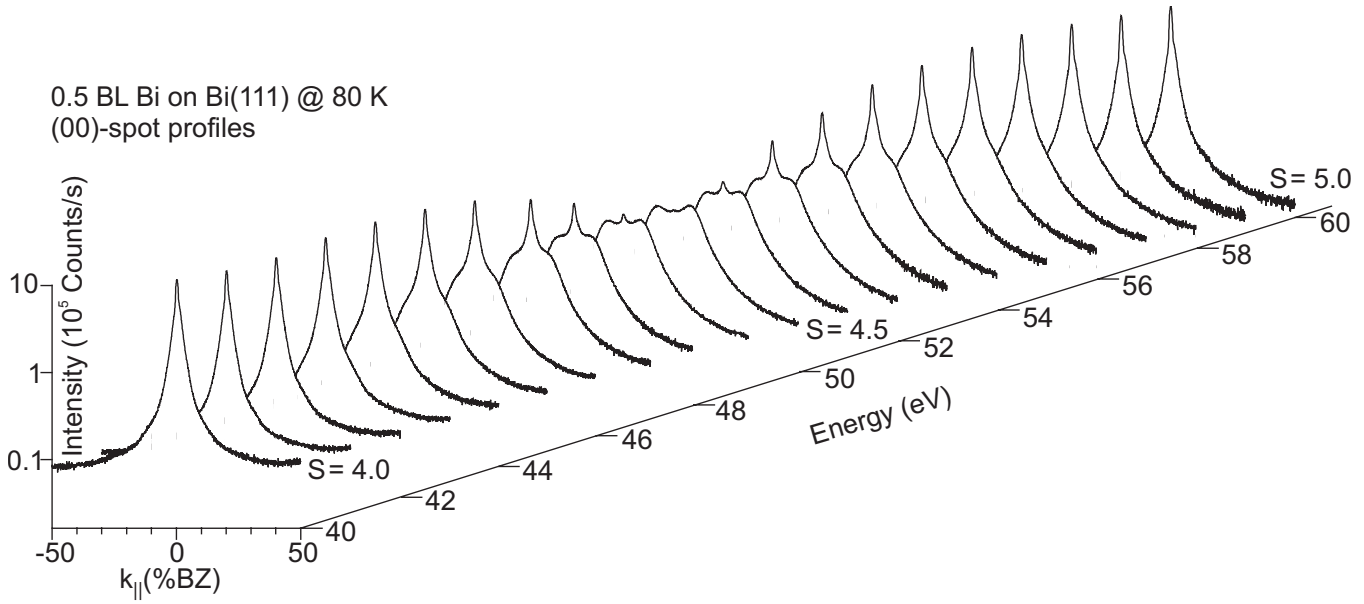

FIG. 4. Variation of the spot profile of (00)-spot with the electron energy E or the scattering phase S recorded after deposition of 0.5 BL Bi on a Bi(111) base film at 80 K. All the profiles are plotted in a logarithmic intensity scale. The profile shows a periodic change from one in-phase scattering condition (S=4) to the next one (S=5). The central spike disappears at the out-of-phase condition (S=4.5) due to destructive interference of the electrons at the 2D islands. The intensity is redistributed to the diffuse intensity of the Henzler ring.

course of deposition of one additional BL. For a coverage of half of a complete BL, the central spike almost vanishes in the minima of the intensity oscillations. Only the diffuse shoulder remains, reflecting the morphological uniformity of the film and maximum surface roughness. The diffuse intensity shows a Henzler ring (see also Fig. 3) indicating a lateral surface roughness with well-defined terrace width distribution. For a complete BL coverage, the central spike shows its maxima and almost no diffuse shoulder indicating a flat surface without lateral roughness.

B. Vertical layer distance

In order to determine the lateral and vertical roughness, i.e., the island size and height we deposited 0.5 BL Bi on a smooth Bi(111) base film at 80 K. The exact coverage was achieved by following the (00)-spot intensity: the first minima correspond to 0.5 BL coverage. The corresponding LEED pattern at out-of-phase condition for the integer order spots is shown in Fig. 3. The quasi-12-fold symmetry originates from the morphology of the Bi(111) base film, which consists of (111) crystallites rotated by 90°. Each of the first-order spots exhibits a pronounced Henzler ring of diffuse intensity with a diameter of $k_{\emptyset}$=17% BZ surrounding a sharp central peak.

The island height is determined from the periodic change of spot profiles with a vertical momentum transfer $k_{\perp}$ or scattering phase S. Therefore, the (00)-spot profile is analyzed over a large range of electron energies—at least from one in-phase condition to the next one. Figure 4 clearly shows how the spot profile varies as a function of the electron energy. At the in-phase condition at 40 eV (S=4), the spot shape is narrow and only shows the instrumental broadening. Here the electrons scattered from neighboring terraces interfere constructively, and therefore, only a sharp peak appears. At the out-of-phase condition at 51 eV (S=4.5), where the electrons from the neighboring terraces interfere destructively, the profile shows the diffuse Henzler ring. The diffuse intensity shows an oscillatory behavior as a function of the electron energy from zero at in-phase condition to a maximum at the out-of-phase condition and to zero at the next in-phase-condition at 61 eV (Fig. 4). The diameter of the Henzler ring, however, remains unchanged with electron energy. This indicates a two-level system with a well-defined distribution of 2D islands with the same height on the surface.[23,37] The change of intensity of the diffuse ring proceeds at the expense of central spike intensity.

In order to eliminate the dynamic form factor of scattering, all spot profiles were normalized by taking the ratio of the integral intensity of the central spike I_{spike} with the total intensity of the spot $I_{\text{total}}=I_{\text{spike}}+I_{\text{diffuse}}$, where I_{diffuse} is the integral intensity of the diffuse shoulder.[22] This normalized central spike intensity is known as $G(S)=I_{\text{spike}}/I_{\text{total}}$ curve and is plotted in Fig. 5 as a function of the square root of the electron energies, i.e., as a function of $k_{\perp}$ or the scattering phase S. The $G(S)$ curve shows an oscillatory behavior with maxima for the in-phase conditions S=3, 4, and 5 and could be well fitted by a cosine function.

For a perfect two-level system (substrate plus islands of the same height), the normalized central spike intensity depends only on the coverage in the first layer θ_1 and oscillates with a cosine function of S as[23,27]

$$G(S) = 1 - 2\theta_1(1 - \theta_1)[1 - \cos(2\pi S)]. \quad (1)$$

In our experiment we have to consider θ_1=0.5 (half of a complete bilayer) and Eq. (1) simplifies to

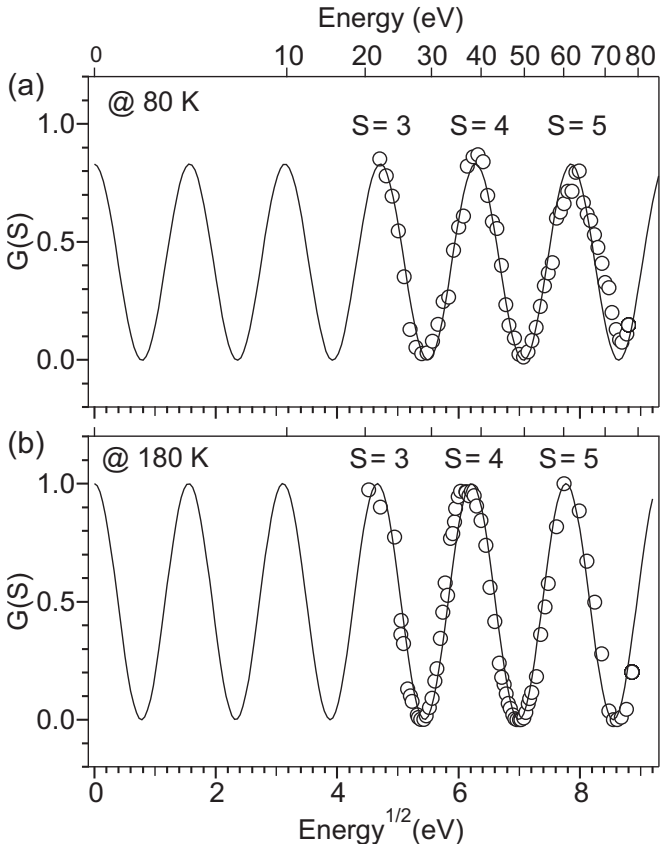

FIG. 5. Normalized central spike intensity $G(S)$ of the LEED (00)-spot profile as a function of S, i.e., the square root of energy. (a) Deposition at 80 K and (b) deposition at 180 K. At in-phase conditions, all the intensity is confined to the central spike due to the constructive interference of the electrons and the $G(S)$ curve shows maxima. At out-of-phase conditions, the central spike vanishes due to the destructive interference and the $G(S)$ curve shows minima. The curves were fitted with the cosine function [Eq. (2)] considering a two-level system and shown with a solid line. We derive an island height of $d_{80\ \mathrm{K}}=0.389$ nm at 80 K and of $d_{180\ \mathrm{K}}=0.395$ nm at 180 K.

$$G(S) = \frac{1}{2}[1 + \cos(2\pi S)], \tag{2}$$

which describes well the observed behavior. If more than two layers are present, higher Fourier components will contribute to the behavior of the $G(S)$ curve.[23,38]

Additionally, from the knowledge of the electron energies of the in-phase conditions and the corresponding scattering phase S, we can determine the island height d via the Laue condition. Constructive interference between adjacent levels is observed for the maxima of the $G(S)$ curve,

$$S = \frac{2d\cos\vartheta}{\lambda_e(E)}, \tag{3}$$

and the Laue condition is fulfilled. Here ϑ is the angle of the incident electron beam with respect to the surface normal ($\cos\vartheta = 0.997 \approx 1$ for the SPA-LEED geometrical construction) and $\lambda_e(E) = h/\sqrt{2m_e eE}$ is the wavelength of the incident electrons, where h is the Planck's constant, e the elementary charge, and E the incident electron energy. From the distance ΔS between two successive maxima or minima of the $G(S)$ curve from the plot in Fig. 5(a) and the respective electron energies, the vertical layer distance can be easily calculated by using the following expression:[23]

$$d = \frac{\Delta S}{2\cos\vartheta}\left[\frac{\lambda_e(E_1)\lambda_e(E_2)}{\lambda_e(E_1) - \lambda_e(E_2)}\right], \tag{4}$$

where $\lambda_e(E_1) = h/\sqrt{2m_e eE_1}$ and $\lambda_e(E_2) = h/\sqrt{2m_e eE_2}$. Using all three in-phase conditions we derive an island height of $d = 0.389 \pm 0.002$ nm, which is close to the bulk Bi lattice plane separation $d_{\mathrm{bulk}} = 0.394$ nm and confirms the previous results of BL step height on Bi(111) films.[10,39] A contraction of $\sim 1\%$ is, however, beyond the error margin that could occur during this measurement. Such a relaxation of the island height is probably caused by a smoothening of the electron-density contours at the edges of the small island (Smoluchowski effect[40]). A similar effect of inward relaxation of the electron contour of the topmost layer has been observed for small Ag islands on Ag(100) by thermal-energy atom scattering (TEAS) analysis.[41] We argue that the effect is more apparent for small islands because the distortion of the electron density at adjacent step edges overlaps leading to an overall smoothening and inward relaxation of the electron-density contour. For large islands, only a negligible contribution of the smoothening effect occurs. In our system, the Bi islands are small (island width $\Gamma < 3$ nm) at 80 K, and it, therefore, has become possible to detect the effect.

The same measurements were performed after depositing 0.5 BL Bi on the Bi(111) base film at 180 K. To avoid any effects of thermal expansion, the data were taken after quenching the film to 80 K. Then the island size is much larger (>10 nm) and the smoothening effect should be smaller. Figure 5(b) shows the $G(S)$ curve, which is similar to the 80 K measurement. The cosine behavior still reflects a two-level system. The location of the maxima, however, is shifted to lower energies, i.e., smaller momentum transfer or larger electron wavelength: the step height is increased to $d = 0.395 \pm 0.002$ nm, which matches almost perfectly the bulk value of $d_{\mathrm{bulk}} = 0.394$ nm within the instrumental error. For these larger islands, we do not observe a contraction in the layer height of the islands. This clearly supports the argument of a smaller contribution of the Smoluchowski smoothening effect for larger islands that might also have been the reason that Bedrossian *et al.*[41] were not able to observe the effect with SPA-LEED because the investigated Ag-islands were rather large ($\Gamma \sim 7$ nm).

C. Lateral roughness

The average island size $\langle\Gamma\rangle$ or island separation $\langle L\rangle$ was determined from the shape of the diffuse part of the spot profile. The dominant central spike is most effectively suppressed for the out-of-phase and half-coverage condition. At 80 K the (00)-spot and the corresponding one-dimensional (1D) spot profile exhibit a typical Henzler ring of diffuse intensity surrounding a sharp central peak (Fig. 3). The observation of a Henzler ring reflects a well-defined size distri-

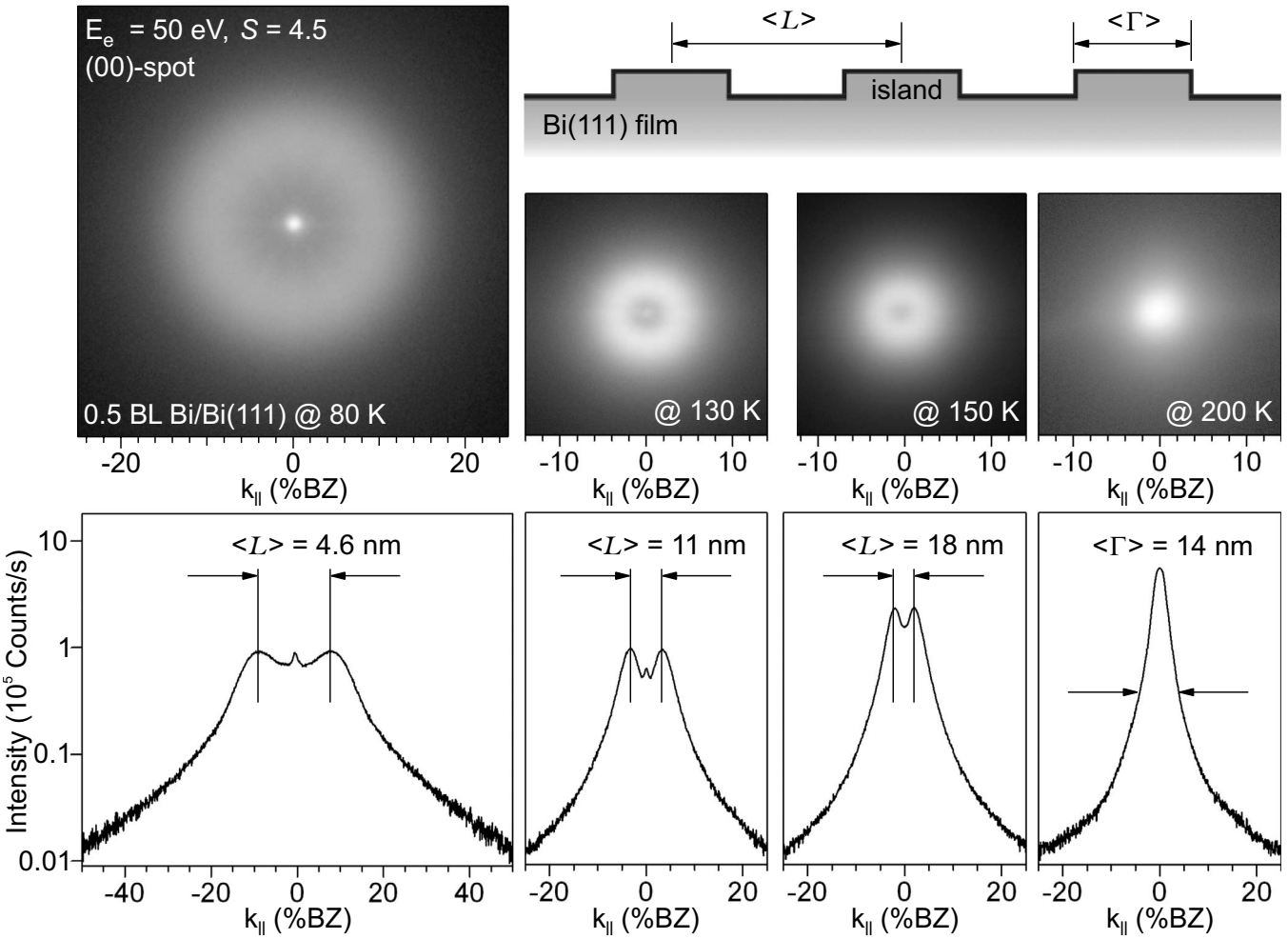

FIG. 6. LEED patterns of (00)-spot and corresponding profiles after deposition of 0.5 BL Bi on the Bi(111) base film at different deposition temperatures. At 80 K, a distinct ring of diffuse intensity—the so called Henzler ring—appears. The diameter of the ring decreases significantly from 80 to 150 K. Finally, at 200 K, a single broadened spot appears. The terrace lengths $\langle L\rangle$ at different deposition temperatures (80–150 K) and the average terrace size $\langle\Gamma\rangle$ at 200 K, as calculated from the 1D spot profile analysis, are shown within the profiles. The cross-section sketch shows Bi islands of average separation $\langle L\rangle$ and average size $\langle\Gamma\rangle$.

bution of regular 2D islands on the surface.[42] The average island separation of $\langle L\rangle = 4.6$ nm is calculated directly from the diameter of the diffuse ring $k_{\varnothing}$ via $\langle L\rangle = 4\pi/k_{\varnothing}$.[42–44] This small value for $\langle L\rangle$ indicates a considerable slow down of mass transport by the existence of an adatom diffusion barrier across the terraces and/or step edges. A higher barrier reduces the adatom diffusion across the terraces and consequently increases the island density n_x, i.e., decreases the average island separation $\langle L\rangle$.

The temperature dependence of the island separation $\langle L\rangle$ was studied by a deposition of 0.5 BL Bi at various temperatures up to 200 K. Immediately after deposition, the sample was cooled down to 80 K to inhibit coarsening of the island distribution. LEED patterns of the (00)-spot and the corresponding spot profiles were recorded at an out-of-phase scattering condition ($S=4.5$) and are shown in Fig. 6.

At higher deposition temperatures, the diameter of the diffuse ring decreases significantly and vanishes completely at 200 K. The decreasing diameter $k_{\varnothing}$ of the Henzler ring in reciprocal space reflects the increasing island separation $\langle L\rangle$, which is equivalent to a decrease in the island density n_x. At 200 K, the island size is so large compared to the instrument response function that the Henzler ring vanishes and a broadened spot remains. Under this condition, the (00)-spot profile gives information about the lateral size of the islands $\langle\Gamma\rangle$ and not the average island separation $\langle L\rangle$. The profile can be fitted well by a Lorentzian function, implying a geometric distribution of islands. The average island size of $\langle\Gamma\rangle = 14$ nm was directly determined from the full width at half maximum (FWHM) κ of the profile by $\langle\Gamma\rangle = 2/\kappa$.[45]

For deposition between 200 and 300 K, we still observe a slight broadening in the spot profile due to build up of small surface roughness. The intensity during deposition as shown in the inset of Fig. 1 clearly exhibits a small decrease even at 300 K. The mobility of the Bi adatoms became that high, in which the growth proceeds via almost step propagation of the preexisting steps of the initial Bi-base film. This trend continues up to 450 K, where the spot profile shows only the instrumental broadening, symbolizing a perfect step propagation growth mode.[11]

Because the (00)-spot provides an average information of the surface morphology, it does not reflect the individual

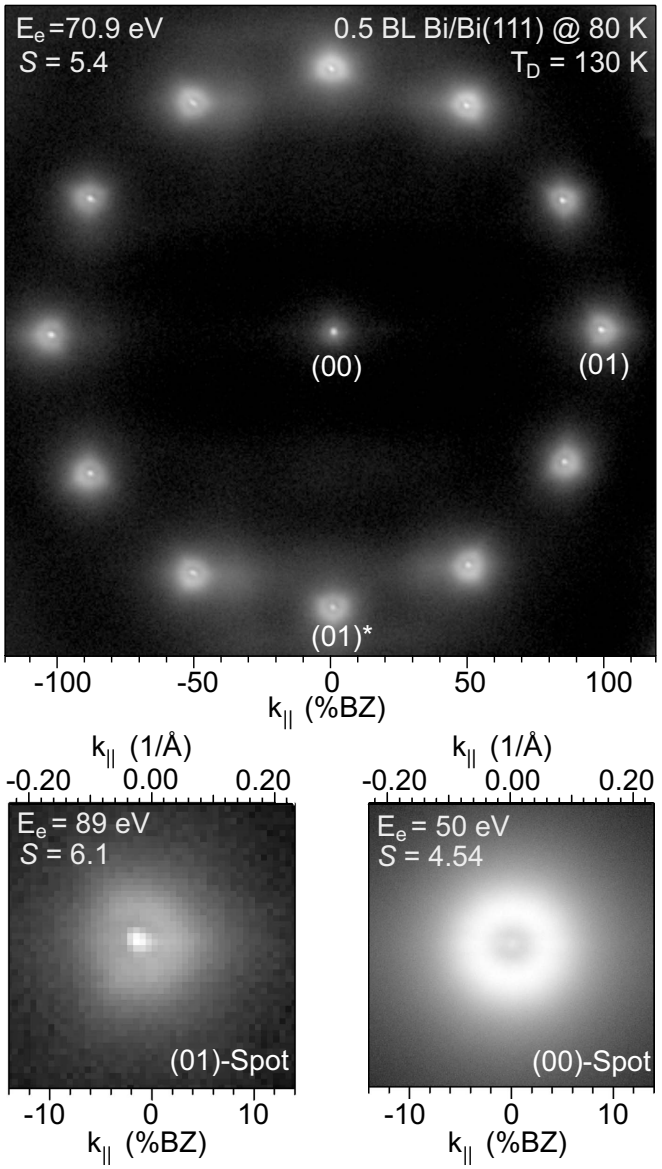

FIG. 7. LEED pattern recorded at an out-of-phase condition (S=5.4) after 0.5 BL Bi deposition on the Bi(111) template film at 130 K. Two different domain spots and the central spot are indicated by (01), (01)*, and (00), respectively. The insets below shows (01) and (00) spots.

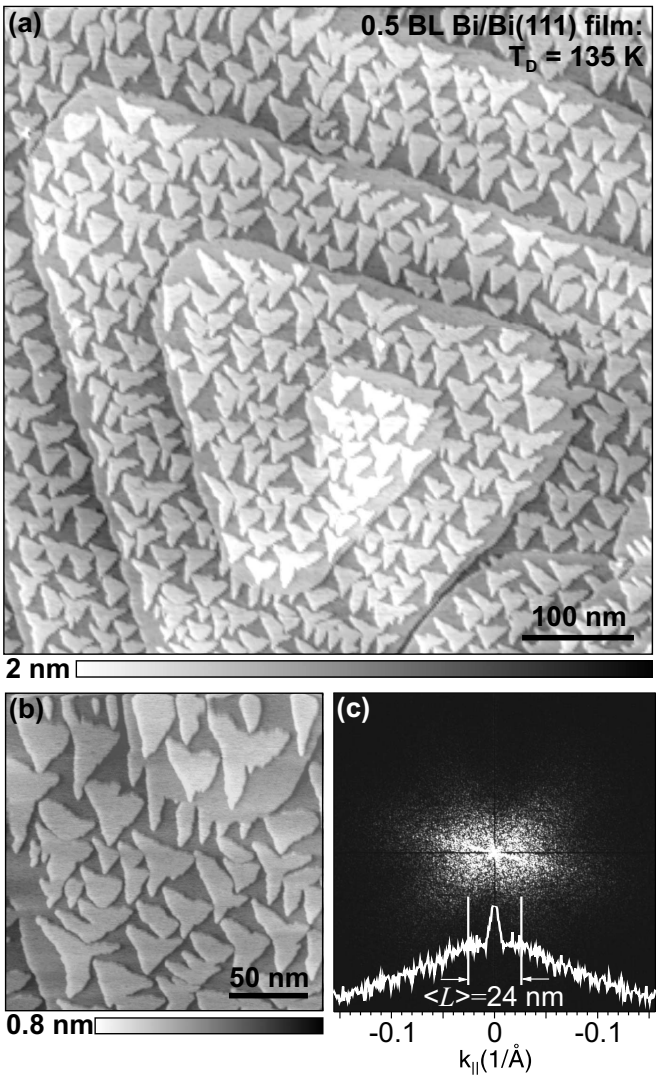

FIG. 8. STM topography (U_{bias}=1.8 V, I_{tunnel}=17 pA) of 0.5 BL Bi grown on the Bi(111) template film at 135 K. (a) The two-dimensional Bi islands of quasidendritic shape are distributed on a highly smooth Bi(111) base film, which exhibits regular step trains of 100 nm separation (which form a growth spiral centered at a screw dislocation). (b) Small region at higher magnification clearly reflects the dendritic shape of the two-dimensional Bi islands. Due to piezocreep, the topmost parts of both STM images appear slightly deformed. (c) The power spectrum of the large STM image (a) shows a Henzler ring. From its spot profile we conclude an average island separation of $\langle L\rangle$=24 nm, which is consistent with the island density of $n_x=2.5\times10^{11}$ cm^{-2}.

shape of the islands. The Bi(111) base film emerges with two rotational domains and two twin domains. Any information about nonisotropic island shapes will be hidden by the incoherent superposition of the individual patterns. This is why the (00)-spots recorded at different deposition temperatures (Fig. 6) all show a circular shaped Henzler ring, while the first-order spots exhibits a clear difference in shape between 80 (Fig. 3) and 130 K (Fig. 7). Because the islands are rather small at 80 K, which are confirmed by the small island separation ($\langle L\rangle$=4.6 nm), LEED cannot resolve the actual shape of the islands. In contrast, at higher deposition temperatures (130–150 K), a threefold symmetry of the first-order LEED spots is observed (Fig. 7). The threefold symmetry spots reflects triangular shaped islands.

For comparison, STM micrographs of 0.5 BL Bi deposited at nominally 135 K were additionally recorded. Figure 8(a) shows 2D triangularlike islands of almost the same size and separation. All islands exhibit a quasidendritic shape as obvious from the higher magnification micrograph in Fig. 8(b). The quasidendritic shape is caused by the asymmetry in diffusion of adatoms from corners to the steps, which occurs generally on a hexagonal surface.[46–48] All islands exhibit the same height of $d\cong0.4$ nm, i.e., a bilayer height. The islands are touching each other. Coalescence and coarsening, however, is not observed. By counting, we determined an island

density of $n_x=2.5\times10^{11}$ cm^{-2}. From this, we estimate an average island separation of $\langle L\rangle=20$ nm.

The power spectrum of the STM micrograph is shown in Fig. 8(c). The profile of the power spectrum also shows a Henzler ring with a diameter of $k_{\varnothing}=0.053$ Å^{-1}, which converts to an average island separation of $\langle L\rangle=24$ nm, which is consistent with the island counting analysis and qualitatively supports the spot profile analysis of the LEED patterns.

D. Surface diffusion energy

Diffusion is a process that is thermally activated and therefore depends strongly on temperature. Thus, the adatom intraterrace diffusion energy can be estimated, based on nucleation theory,[15] by an analysis of the island density as a function of growth temperature. According to nucleation theory, the growth proceeds via three kinetic regimes as function of coverage θ. The adatom density increases with θ at the very beginning of the nucleation process until the first stable nuclei are formed and the island separation becomes comparable to the adatom diffusion length. This regime is known as the nucleation regime with the formation of a stable island density, n_x. Then the adatom density suddenly drops because they are trapped by existing islands, which behave like a sink. In this aggregation regime, the system is in a quasi-steady-state, which continues up to the coalescence regime where islands touch each other and merge. Upon further deposition, the island density n_x ultimately reduces to zero as the first layer is completed.

The rate-equation estimates the island density n_x in the aggregation regime as[14,15,26]

$$n_x(r,T) \propto r^p \exp\left(\frac{E_n}{k_BT}\right), \tag{5}$$

where r denotes the deposition rate, E_n the characteristic energy, k_B the Boltzmann constant, and T the deposition temperature. The parameter p is a scaling parameter, which is determined by the number i of adatoms required for the stable nuclei. The parameters E_n and p are given by

$$p=\frac{i}{i+2}, \quad E_n=\frac{E_i+iE_d}{i+2}. \tag{6}$$

Here, E_i is the binding energy of an atom within the critical nucleus and E_d is the intraterrace diffusion energy. Assuming that the size of the critical nucleus is one, i.e., $i=1$, which corresponds to $E_i=0$,[49] the Eq. (5) can be simplified to

$$n_x(r,T) \propto r^{1/3} \exp\left(\frac{E_d}{3k_BT}\right). \tag{7}$$

For the submonolayer quasi-steady-state regime, where the island size grows with coverage,[42] the average island separation depends directly on the island density via $\langle L\rangle \sim n_x^{-1/2}$.[25] Because, for each deposition temperature, a constant deposition rate has been used, the rate equation in Eq. (7) can be rearranged as

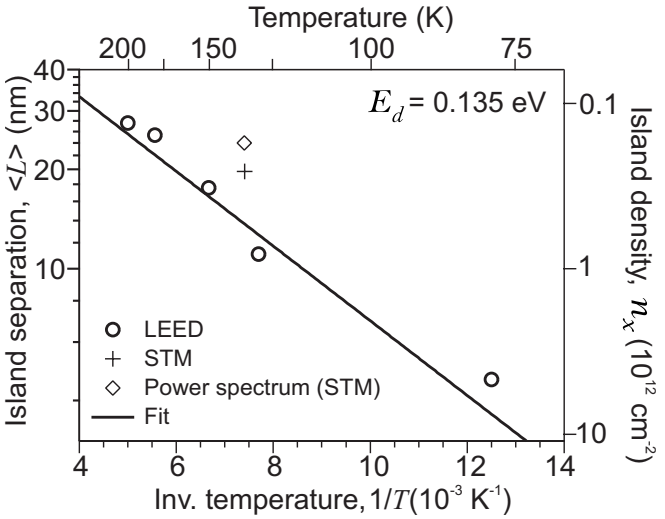

FIG. 9. Arrhenius plot of the average island separation $\langle L\rangle$ and the island density n_x for 0.5 BL Bi on Bi(111) base film deposited at different temperatures T (80–200 K). The measured curve is fitted employing Eq. (8), where the slope of the fit gives an intraterrace diffusion energy of $E_d=0.135$ eV.

$$\langle L\rangle \propto \exp\left(-\frac{E_d}{6k_BT}\right). \tag{8}$$

From the Arrhenius plot of Eq. (8), which is shown in Fig. 9, the intraterrace diffusion energy of $E_d=0.135$ eV was determined. The island density and the average island separation obtained from the STM image and the corresponding power spectrum for 135 K (Fig. 8) were not considered. However, the values are very close to the fit within an error of data evaluation, showing a qualitative agreement.

In general, the value $E_d=0.135$ eV is far lower as compared to metal(100) homoepitaxial systems and fairly comparable to metal(111) systems.[50,51] However, exceptionally, as in the Pt/Pt(111) system,[52,53] a weak *Ehrlich-Schwoebel* step edge barrier and asymmetric dendritic shaped islands might be the dominant factors associated with the smooth growth of Bi(111), even at low temperatures.

IV. CONCLUSION

We studied the homoepitaxial growth of Bi(111) by a SPA-LEED and STM in the regime of kinetic limitations, i.e., temperatures between 80 and 300 K. Bi grows in a quasi bilayer-by-bilayer mode as evident from long lasting LEED intensity oscillations during deposition. From the slow kinetic roughening of the growth front, we conclude the existence of a weak *Ehrlich-Schwoebel* step edge barrier for interlayer diffusion across step edges. Above 300 K step propagation is observed, resulting in terrace widths of more than 100 nm.

All steps and 2D islands on the Bi(111) surface exhibit exclusively a bilayer height of $d_{\mathrm{Bi(111)}}=0.394$ nm, i.e., the triple dangling bond termination of the Bi(111) is unstable and only the single dangling bond termination is observed. The size of the 2D islands varies from $\langle\Gamma\rangle=3$ nm at 80 K up

to $\langle\Gamma\rangle = 15$ nm at 200 K. From this we estimate an activation energy for intralayer diffusion of $E_d = 0.135$ eV, which is comparable to values typically observed for metal homoepitaxy. At intermediate temperatures, the 2D islands exhibit a threefold dendritic shape due to kinetic limitations of edge diffusion. Bulk defect formation in the Bi-film as stacking faults, twins, or dislocations were not observed. At elevated temperatures of 450 K, very smooth Bi(111) surfaces could be obtained during homoepitaxial growth with a terrace width exceeding 400 nm.[11,13]

ACKNOWLEDGMENTS

Financial support from the Deutsche Forschungsgemeinschaft through SFB 616 "Energy Dissipation at Surfaces" is gratefully acknowledged.

*gr.jnawali@uni-due.de
†Present address. Department of Physics and Astronomy and Department of Chemistry, University of California Irvine, California 92697-4575, USA.

[1] J. P. Issi, Aust. J. Phys. **32**, 585 (1979).
[2] F. Y. Yang, K. Liu, K. Hong, D. H. Reich, P. C. Searson, and C. L. Chien, Science **284**, 1335 (1999).
[3] G. A. Prinz, Science **282**, 1660 (1998).
[4] Y. M. Koroteev, G. Bihlmayer, J. E. Gayone, E. V. Chulkov, S. Blügel, P. M. Echenique, and P. Hofmann, Phys. Rev. Lett. **93**, 046403 (2004).
[5] Ph. Hofmann, Prog. Surf. Sci. **81**, 191 (2006).
[6] T. Hirahara, T. Nagao, I. Matsuda, G. Bihlmayer, E. V. Chulkov, Y. M. Koroteev, P. M. Echenique, M. Saito, and S. Hasegawa, Phys. Rev. Lett. **97**, 146803 (2006).
[7] T. Hirahara, T. Nagao, I. Matsuda, G. Bihlmayer, E. V. Chulkov, Y. M. Koroteev, and S. Hasegawa, Phys. Rev. B **75**, 035422 (2007).
[8] T. Hirahara, I. Matsuda, S. Yamazaki, N. Miyata, and S. Hasegawa, Appl. Phys. Lett. **91**, 202106 (2007).
[9] M. Kammler and M. Horn-von Hoegen, Surf. Sci. **576**, 56 (2005).
[10] T. Nagao, J. T. Sadowski, M. Saito, S. Yaginuma, Y. Fujikawa, T. Kogure, T. Ohno, Y. Hasegawa, S. Hasegawa, and T. Sakurai, Phys. Rev. Lett. **93**, 105501 (2004).
[11] G. Jnawali, H. Hattab, B. Krenzer, and M. Horn von Hoegen, Phys. Rev. B **74**, 195340 (2006).
[12] G. Jnawali, H. Hattab, F. J. Meyer zu Heringdorf, B. Krenzer, and M. Horn-von Hoegen, Phys. Rev. B **76**, 035337 (2007).
[13] H. Hattab, E. Zubkov, A. Bernhart, G. Jnawali, C. Bobisch, B. Krenzer, M. Acet, R. Möller, and M. Horn-von Hoegen, Thin Solid Films (in press).
[14] J. A. Venables, Philos. Mag. **27**, 697 (1973).
[15] J. A. Venables, G. D. T. Spillert, and M. Hanbücken, Rep. Prog. Phys. **47**, 399 (1984).
[16] L. Bardotti, C. R. Stoldt, C. J. Jenks, M. C. Bartelt, J. W. Evans, and P. A. Thiel, Phys. Rev. B **57**, 12544 (1998).
[17] G. L. Kellogg, Surf. Sci. Rep. **21**, 1 (1994).
[18] H. Brune, H. Röder, C. Boragno, and K. Kern, Phys. Rev. Lett. **73**, 1955 (1994).
[19] J. A. Stroscio, D. T. Pierce, and R. A. Dragoset, Phys. Rev. Lett. **70**, 3615 (1993).
[20] M. Stanley, C. Papageorgopoulos, K. R. Roos, and M. C. Tringides, Surf. Sci. **355**, L264 (1996).
[21] A. Fissel, M. Oehme, K. Pfennighaus, and W. Richter, Surf. Sci. **383**, 370 (1997).
[22] M. Horn and M. Henzler, J. Cryst. Growth **81**, 428 (1987).
[23] M. Horn-von Hoegen, Z. Kristallogr. **214**, 591 (1999).
[24] M. Horn-von Hoegen and H. Pietsch, Surf. Sci. **321**, L129 (1994).
[25] G. Meyer, J. Wollschläger, and M. Henzler, Surf. Sci. **231**, 64 (1990).
[26] J. A. Venables, Surf. Sci. **299/300**, 798 (1994).
[27] U. Scheithauer, G. Meyer, and M. Henzler, Surf. Sci. **178**, 441 (1986).
[28] D. J. Chadi, Phys. Rev. Lett. **43**, 43 (1979).
[29] T. Tabaka, T. Aruga, and Y. Murata, Surf. Sci. **179**, L63 (1987).
[30] R. A. Wolkow, Phys. Rev. Lett. **68**, 2636 (1992).
[31] K. Inoue, Y. Morikawa, K. Terakura, and M. Nakayama, Phys. Rev. B **49**, 14774 (1994).
[32] J. Wollschläger, Th. Schmidt, M. Henzler, and M. I. Larsson, Surf. Sci. **454-456**, 566 (2000).
[33] W. F. Egelhoff, Jr. and I. Jacob, Phys. Rev. Lett. **62**, 921 (1989).
[34] M. Horn-von Hoegen, J. Falta, and M. Henzler, Thin Solid Films **183**, 213 (1989).
[35] G. Ehrlich and F. G. Hudda, J. Chem. Phys. **44**, 1039 (1966).
[36] R. L. Schwoebel and E. J. Shipsey, J. Appl. Phys. **37**, 3682 (1966).
[37] C. S. Lent and P. I. Cohen, Surf. Sci. **139**, 121 (1984).
[38] R. Altsinger, H. Busch, M. Horn, and M. Henzler, Surf. Sci. **200**, 235 (1988).
[39] V. Edel'man, Phys. Lett. A **210**, 105 (1996).
[40] R. Smoluchowski, Phys. Rev. **60**, 661 (1941).
[41] P. Bedrossian, B. Poelsema, G. Rosenfeld, L. C. Jorritsma, N. N. Lipkin, and G. Cosma, Surf. Sci. **334**, 1 (1995).
[42] P. Hahn, J. Clabes, and M. Henzler, J. Appl. Phys. **51**, 2079 (1980).
[43] M. Henzler, Appl. Surf. Sci. **11-12**, 450 (1982).
[44] J. K. Zuo, J. F. Wendelken, H. Dürr, and C. L. Liu, Phys. Rev. Lett. **72**, 3064 (1994).
[45] E. Z. Luo, J. Wollschläger, F. Wegner, and M. Henzler, Appl. Phys. A: Mater. Sci. Process. **60**, 19 (1995).
[46] K. Stolt, W. R. Graham, and G. Ehrlich, J. Chem. Phys. **65**, 3206 (1976).
[47] Th. Michely and G. Cosma, Surf. Sci. **256**, 217 (1991).
[48] M. Hohage, M. Bott, M. Morgenstern, Z. Zhang, Th. Michely, and G. Comsa, Phys. Rev. Lett. **76**, 2366 (1996).
[49] A variation of the deposition rate would allow to independently determine also the size of the critical nucleus i. Such an experiment, however, is very challenging and is beyond the focus of this work. (see Ref. 24 also).
[50] P. Stoltze, J. Phys.: Condens. Matter **6**, 9495 (1994).
[51] C.-M. Zhang, M. C. Bartelt, J.-M. Wen, C. J. Jenks, J. W. Evans, and P. A. Thiel, Surf. Sci. **406**, 178 (1998).
[52] J. Jacobsen, K. W. Jacobsen, P. Stoltze, and J. K. Nørskov, Phys. Rev. Lett. **74**, 2295 (1995).
[53] K. Kyuno and G. Ehrlich, Phys. Rev. Lett. **81**, 5592 (1998).